

Coherent instabilities in a semiconductor laser with fast gain recovery

Christine Y. Wang,¹ L. Diehl,² A. Gordon,³ C. Jirauschek,³ F. X. Kärtner,^{3,*} A. Belyanin,⁴ D. Bour,⁵ S. Corzine,⁵ G. Höfler,⁵ M. Troccoli,² J. Faist,⁶ and Federico Capasso^{2,†}

¹*Department of Physics, Harvard University, Cambridge, Massachusetts 02138, USA*

²*School of Engineering and Applied Science, Harvard University, Cambridge, Massachusetts 02138, USA*

³*Department of Electrical Engineering and Computer Science and Research Laboratory of Electronics, Massachusetts Institute of Technology, 77 Massachusetts Avenue, Cambridge, Massachusetts 02139, USA*

⁴*Department of Physics, Texas A & M University, College Station, Texas 77843, USA*

⁵*Agilent Technologies, Palo Alto, California 94306, USA*

⁶*Institute of Physics, University of Neuchâtel, CH-2000 Neuchâtel, Switzerland*

(Received 11 July 2006; published 30 March 2007)

We report the observation of a coherent multimode instability in quantum cascade lasers (QCLs), which is driven by the same fundamental mechanism of Rabi oscillations as the elusive Risken-Nummedal-Graham-Haken (RNGH) instability predicted 40 years ago for ring lasers. The threshold of the observed instability is significantly lower than in the original RNGH instability, which we attribute to saturable-absorption nonlinearity in the laser. Coherent effects, which cannot be reproduced by standard laser rate equations, can play therefore a key role in the multimode dynamics of QCLs, and in lasers with fast gain recovery in general.

DOI: [10.1103/PhysRevA.75.031802](https://doi.org/10.1103/PhysRevA.75.031802)

PACS number(s): 42.55.Px, 42.60.Mi, 42.65.Sf

The fundamental coherent mechanism that can destabilize a single-mode laser was predicted in the early 1960s [1] and was later extended to multimode lasers [2,3] where it became known as the Risken-Nummedal-Graham-Haken (RNGH) instability. These instabilities became classic landmarks for the general field of nonlinear dynamics [4,5] because they emerge in conceptually the simplest laser model, which in the single-mode case was shown to be equivalent to the Lorenz model of deterministic chaos [6]. Another feature that makes these instabilities so interesting and unique is their coherent nature that involves the polarization of the medium as a nontrivial dynamical variable. Most other physical mechanisms that can drive a laser from a single-mode to a multimode regime, such as spatial and spectral hole burning, Q switching, and saturable absorption [7,8], can be adequately described within the standard rate equation formalism, in which the polarization of the active medium is adiabatically eliminated. Both the single mode [1] and the multimode [2,3] instabilities cannot be explained by the rate equations. Such coherent effects can be only observed when the polarization is driven faster than or on a time scale comparable to the dephasing time T_2 [9].

The origin of the two coherent phenomena mentioned above is the oscillation of the population inversion at the Rabi frequency Ω_{Rabi} that takes place when the intracavity laser intensity becomes large. This results in a modification of the gain spectrum and the emergence of sidebands separated from the maximum of the gain curve by an amount corresponding to the Rabi frequency. These sidebands can be regarded as a manifestation of parametric gain. The instability sets in when the intracavity power is sufficiently large: the Rabi angular frequency Ω_{Rabi} has to be greater than the relaxation time scales of the gain medium [more precisely,

Ω_{Rabi} is sufficiently greater than $(T_1 T_2)^{-1/2}$, where T_1 is the gain relaxation time]. The instability threshold is often called the second laser threshold due to its universal nature.

Pioneering theoretical works stimulated extensive experimental studies that finally resulted in the observation of the Lorenz-type chaos in a far-infrared single-mode laser [10]. However, despite almost 40 years of efforts, the experimental demonstration of the multimode RNGH instability has remained somewhat controversial [11–16].

In lasers with long gain recovery compared to the cavity round-trip time, the instability caused by a saturable absorber can often lead to mode locking [8]. When the gain recovery time is short compared with the cavity round-trip time, it is usually assumed that the laser dynamics becomes very primitive and uninteresting (so-called class A laser). In this case mode locking is impossible according to conventional theory, and the relaxation oscillation frequency becomes purely imaginary [17]. Surprisingly, as we show in this Rapid Communication, it is under these conditions that the elusive RNGH instability can be observed. We show that quantum cascade lasers (QCLs) are uniquely suited for studying these coherent effects which, along with spatial hole burning (SHB), become a key factor in dictating the dynamics of the laser.

QCLs, because they are based on ultrafast tunneling and phonon-limited intersubband transitions, belong to the class of lasers which have an extremely fast gain recovery, in the range of a few ps [18]. Recent experiments showed indeed that the gain recovers within a few ps, which is approximately an order of magnitude shorter than the cavity round-trip time [19]. Since its invention in 1994, QCLs have undergone tremendous improvement [20]. Recent development of low loss, high power QCLs [21,22] enables the study of previously under investigated aspects, such as the richness of the optical spectrum and the ultrafast dynamics of these devices. In Ref. [23], strong evidence of self-pulsations at the cavity round-trip frequency was reported in QCLs, in par-

*Electronic address: kaertner@mit.edu

†Electronic address: capasso@deas.harvard.edu

ticular a large broadening of the spectrum above the threshold of this instability was observed. However, no detailed pulse characterization was provided. The technological potential of QCLs calls for a better understanding of the interplay of various instabilities in the parameter regime dictated by these lasers. Moreover, the Rabi frequency in QCLs at the power levels of a few hundred mW is of the order of a few THz, much larger than the spacing of Fabry-Perot modes. Therefore coherent effects should be easily observable in QCLs.

In this Rapid Communication we present a clear experimental demonstration of a coherent instability, driven by the same mechanism as the RNGH instability. It is identified in the most direct manner, by demonstrating in the optical spectrum of QCLs a splitting corresponding to twice the Rabi frequency.

The instability observed differs in some aspects from the original RNGH instability [2,3]. The threshold of instability can be as low as a few tens of percent above the laser threshold, as shown in Fig. 1(a). In addition, the pure RNGH instability typically gives rise to spectra with one central mode and two sidebands separated from it by the Rabi frequency, whereas in our experiments we observed two peaks only, similarly to Ref. [11]. However, the mechanism of the instability is the same in essence, namely the Rabi oscillations of the population inversion due to coherent effects. The differences from the RNGH instability as it occurs in ideal conditions [2,3] can be attributed to the presence of saturable absorption and SHB.

The QCLs studied were fabricated from two different wafers (wafer nos. 3251 and 3252) grown by metalorganic vapor phase epitaxy. The devices were processed into buried heterostructure lasers, in which an insulating Fe-doped InP layer is regrown after etching of the ridges [21,22]. The active region of all the samples tested is based on a four-quantum-well design, which relies on a double phonon resonance to achieve population inversion [24]. Note, however, that the multimode operation described in the present paper was also observed with lasers based on so-called three-quantum-well designs [18]. Figure 1(a) shows the optical spectra of a laser operated in continuous wave (cw) at room temperature. The active region of this laser is 3 μm wide and its emission wavelength is close to 8.47 μm (wafer no. 3251). The laser was cleaved into a 3-mm-long bar and soldered with indium onto a copper heat sink. The spectra were measured by a Fourier transform infrared spectrometer (FTIR) equipped with a deuterated triglycine sulphate (DTGS) detector.

As shown in Fig. 1(a), the laser spectrum is single mode close to threshold and broadens as the pumping current increases, splitting into two separated humps. The difference between the weighted centers of the two peaks increases linearly as a function of the square root of the collected output power from one facet, as shown in Fig. 1(b) (square dots with the dashed line as its best fit). The Rabi angular frequency Ω_{Rabi} can be easily calculated using the formula $\Omega_{\text{Rabi}} = \mu E / \hbar = \mu \sqrt{2n I_{\text{ave}}} / (c \epsilon / \hbar)$, where μ is the electron charge times the matrix element of the laser transition ($=2.54$ nm). I_{ave} is the average intracavity intensity in the gain region, which can be derived from the measured output

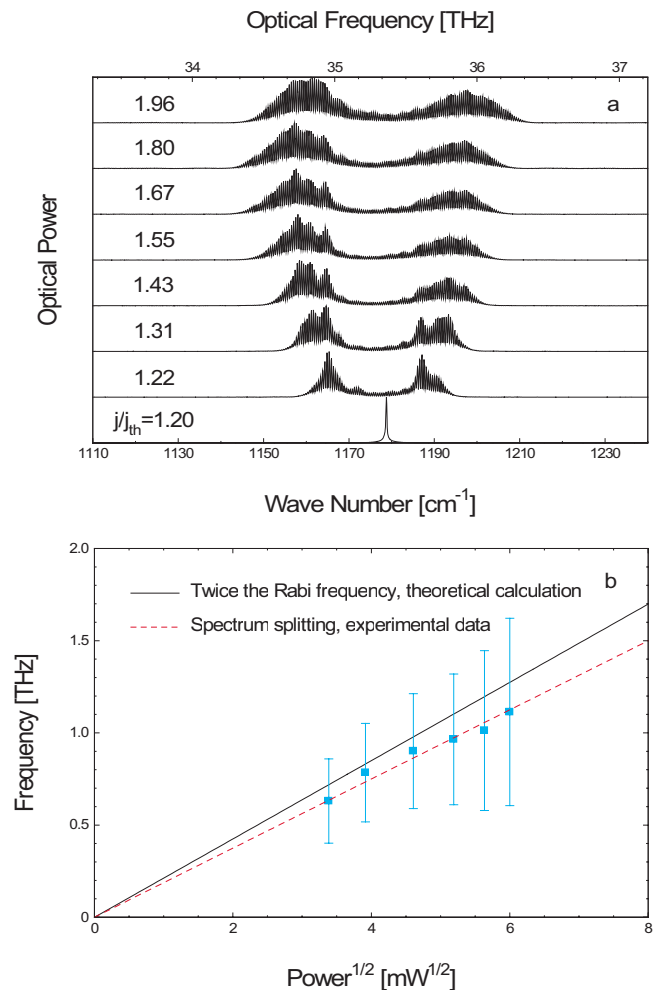


FIG. 1. (Color online) (a) Optical spectra vs pumping ratio (j/j_{th}) above threshold obtained in cw at 300 K with a 3- μm -wide buried heterostructure lasers emitting at 8.47 μm . For $1 < j/j_{\text{th}} < 1.2$ the spectra are identical to $j/j_{\text{th}} = 1.2$. (b) Spectral splitting and twice the Rabi frequency $\Omega_{\text{Rabi}}/(2\pi)$ vs square root of output power collected from a single laser facet. The different quantities reported on the graph were deduced from the experimental data shown in (a). The dashed line is a least-square linear fit of the data.

power. c is the speed of light in vacuum and n is the background refractive index. For all the values of the intensity corresponding to the spectra reported in Fig. 1(a), Ω_{Rabi} was calculated, multiplied by a factor 2 and then added to Fig. 2(b) (solid line). A very good agreement is found between the experimental splitting and twice the estimated Rabi frequency. Both curves fall indeed well within the error bars [25]. As mentioned before, the theory behind the RNGH instability predicts that the large intracavity intensity will result in parametric gain at frequencies detuned from the maximum of the gain curve by the Rabi frequency. The agreement mentioned above is thus a strong indication of the RNGH instability in QCLs.

In order to better understand the experimental spectra of the QCLs presented in Fig. 1(a), we use a simple model based on the standard one-dimensional Maxwell-Bloch equations [9], where the active medium is described by an “open” two-level system [26]. However, contrary to the standard

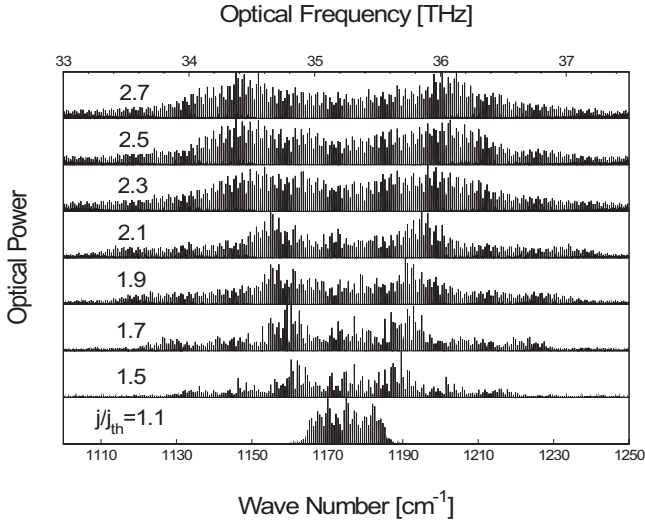


FIG. 2. Results of numerical simulations of the spectra based on the Maxwell-Bloch equations including a saturable absorber and spatial hole burning for different values of the current density normalized to the threshold value.

unidirectional Maxwell-Bloch equations, we allow the electromagnetic field to propagate in both directions. The waves traveling in the two directions are coupled, as they share the same gain medium. This gives rise to SHB [7]: The standing wave formed by a cavity mode imprints a grating in the gain medium through gain saturation. As a result, other modes become more favorable for lasing, and a multimode operation is triggered.

In the slowly varying envelope approximation, the equations read

$$\frac{n}{c} \partial_t E_{\pm} = \mp \partial_z E_{\pm} - i \frac{kN\mu\Gamma}{2\epsilon_0 n^2} \eta_{\pm} - \frac{1}{2} \ell(E_+, E_-) E_{\pm}, \quad (1a)$$

$$\partial_t \eta_{\pm} = \frac{i\mu}{2\hbar} (\Delta_0 E_{\pm} + \Delta_2^{\pm} E_{\mp}) - \frac{\eta_{\pm}}{T_2}, \quad (1b)$$

$$\partial_t \Delta_0 = \frac{\Delta_p - \Delta_0}{T_1} + \frac{i\mu}{\hbar} (E_+^* \eta_+ + E_-^* \eta_- - \text{c.c.}), \quad (1c)$$

$$\partial_t \Delta_2^{\pm} = \pm i \frac{\mu}{\hbar} (E_+^* \eta_- - \eta_+^* E_-) - \frac{\Delta_2^{\pm}}{T_1}. \quad (1d)$$

The + and - subscripts label the two directions of propagation. E and η are the slowly varying envelopes of the electric field and the polarization, respectively. The actual electric field and polarization are obtained by multiplying E and η by $e^{i\omega t}$ (ω is the optical resonance frequency) and taking the real part. The position-dependent inversion is written as the sum of the three terms, Δ_0 , $\Delta_2^+ e^{2ikz}$, and $\Delta_2^- e^{-2ikz}$, where $(\Delta_2^+)^* \equiv \Delta_2^-$. The inversion is thereby represented by two slowly varying functions (Δ_0 and Δ_2^+), and $e^{\pm 2ikz}$ gives the fast variation in space. All the quantities mentioned so far are functions of space z and time t .

$\ell(E_+, E_-)$ is the loss in the cavity (not including the mirror loss), which is allowed to be nonlinear and dependent on the intensity. In this work we assume

$$\ell(E_+, E_-) = \ell_0 - \gamma(|E_+|^2 + |E_-|^2), \quad (2)$$

where ℓ_0 is the linear loss and γ is the self-amplitude modulation coefficient characterizing the nonlinear (saturable) part of the loss. Such a saturable absorption mechanism can come from Kerr lensing [8,23], caused by a nonlinear refractive index n_2 in the active region. As the intensity increases, the mode is more confined in the plane transverse to the propagation direction, and the net gain it experiences is greater. The reason is twofold: First, the mode overlaps more with the active region, leading to a larger modal gain (this mechanism is often called “soft Kerr lensing” [27]). Second, the overlap with the metal contacts is smaller, leading to smaller losses [23].

E_+ and E_- satisfy the boundary conditions $E_+ = rE_-$ at the $z=0$ boundary and $rE_+ = E_-$ at the $z=L$ boundary (L is the cavity length and $r \approx 0.53$ is the reflection coefficient). The other quantities in Eq. (1) are constants: k , N , and Γ are the wave number (in the material) associated with the resonance optical frequency, the electron density in the active region, and the overlap factor between the laser mode and the active region, respectively.

Figure 2 shows spectra that were obtained by solving numerically Eqs. (1) with the following parameters: for the saturable absorber, we used $\gamma = 10^{-8} \frac{\text{cm}}{\text{V}^2}$, obtained from two-dimensional mode simulations, assuming a $n_2 \approx 10^{-9} \frac{\text{cm}^2}{\text{W}}$ [23]. The index change due to this n_2 at typical intracavity intensities is about 10^{-3} . The other parameters are $\ell_0 = 5 \text{ cm}^{-1}$, $T_1 = 0.5 \text{ ps}$ [19], $T_2 = 0.07 \text{ ps}$ (corresponding to a gain full width at half maximum bandwidth of 4.8 THz), $L = 0.3 \text{ cm}$, and $n = 3$, which are typical values for these lasers. N and Γ are not needed as long as the pumping is expressed relative to the lasing threshold. Note that the simulated spectra presented in Fig. 2 are averaged over about a microsecond. Only then does the average spectrum reach a steady state and a clear pattern shows up. The averaging is motivated by the fact that experimentally the spectra are acquired over an even much longer time scale. The envelopes of the spectra show two clear peaks whose separation compares well with twice the Rabi frequency, similarly to the experiment.

The lowering of the RNGH instability threshold by a saturable absorber can be established analytically by means of linear stability analysis. We propose this mechanism as the main reason for the observation of the RNGH instability at much lower pumping than RNGH theory predicts. In order to support this idea, we now present spectra from another device similar to the one described previously. The only difference between the two lasers is a shorter optical wavelength ($5.25 \mu\text{m}$) (wafer no. 3252) and a wider active region ($5 \mu\text{m}$). The two-dimensional waveguide simulations indicate a much weaker Kerr-lensing effect in these QCLs (γ is smaller by a factor of 4), due to the much larger ratio of active region width to wavelength. The measured optical spectra obtained at 300 K in cw mode with the $5\text{-}\mu\text{m}$ device

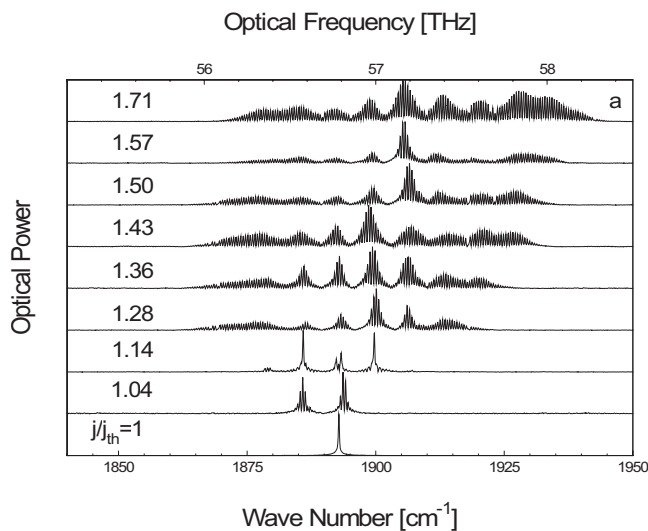


FIG. 3. Optical spectra vs pumping ratio above threshold obtained in cw at 300 K with a $5\text{-}\mu\text{m}$ -wide buried heterostructure lasers emitting at $5.25\ \mu\text{m}$.

are shown in Fig. 3. The data clearly show that the laser is at first single mode close to threshold and becomes multimode immediately after a slight increase of the pumping current. The envelopes of the spectra consist of multiple peaks, with an average separation $0.2\ \text{THz}$, independently of the pumping. Numerical integration of Eq. (1) without a saturable absorber ($\gamma=0$) leads to spectra that qualitatively agree with the ones in Fig. 3.

Reference [15] suggested that the suppression of the central peak in RNGH-type spectra can be due to the complex

level structure of the gain medium, a dye molecule in that case. We show that SHB can also result in the suppression of the central peak (Fig. 2).

Our postulation of saturable absorption due to Kerr-lensing is supported by more extensive study of different devices beyond those shown in this Rapid Communication. First, we observed that for the same emission wavelength, a broad active region leads to a less pronounced RNGH-type signature. Second, we have also tested several standard ridge waveguide QCLs, for which the sidewalls of the ridges are covered by the gold contact. For these devices the coupling between the optical mode and the metal is expected to be stronger and so is the effect of saturable absorber due to Kerr lensing. The spectral behavior observed in this class of devices is dominated by RNGH-type instability.

In summary, a coherent multimode instability in quantum cascade lasers (QCLs) has been observed. It is similar in many ways to the Risken-Nummedal-Graham-Haken (RNGH) instability. The threshold of the observed phenomenon is significantly lower than in the original RNGH instability, which is attributed to the presence of a saturable absorber in the laser. For devices with a weaker saturable absorber, the envelope of the optical spectrum consists of many maxima whose separations are independent of the intracavity power. The nontrivial shape of the spectrum can be explained by SHB.

Support from the U.S. Army Research Laboratory and the U.S. Army Research Office under Grant No. W911NF-04-1-0253 is gratefully acknowledged. Part of the device processing was done at the Center for Nanoscale Systems (CNS) at Harvard University. Harvard-CNS is a member of the National Nanotechnology Infrastructure Network (NNIN).

-
- [1] A. Z. Grasiuk and A. N. Oraevsky, *Proceedings of the VI International Congress on Microwave Tubes*, Scheveningen, Holland, 1962.
- [2] H. Risken and K. Nummedal, *J. Appl. Phys.* **39**, 4662 (1968).
- [3] P. Graham and H. Haken, *Z. Phys.* **213**, 420 (1968).
- [4] H. Haken, *Synergetics* (Springer, New York, 1983).
- [5] Ya. I. Khanin, *Principles of Laser Dynamics* (North-Holland, Amsterdam, 1996).
- [6] H. Haken, *Phys. Lett.* **53A**, 77 (1975).
- [7] A. Yariv, *Quantum Electronics*, 3rd ed. (John Wiley and Sons, New York, 1989).
- [8] H. A. Haus, *IEEE J. Sel. Top. Quantum Electron.* **6**, 1173 (2000).
- [9] L. Allen and J. H. Eberly, *Optical Resonance and Two Level Atoms* (Dover, New York, 1987).
- [10] C. O. Weiss and J. Brock, *Phys. Rev. Lett.* **57**, 2804 (1986).
- [11] L. W. Hillman, J. Krasinski, R. W. Boyd, and C. R. Stroud, Jr., *Phys. Rev. Lett.* **52**, 1605 (1984).
- [12] E. H. M. Hogenboom, W. Klische, C. O. Weiss, and A. Godone, *Phys. Rev. Lett.* **55**, 2571 (1985).
- [13] E. M. Pessina, G. Bonfrate, F. Fontana, and L. A. Lugiato, *Phys. Rev. A* **56**, 4086 (1997).
- [14] T. Voigt, M. O. Lenz, F. Mitschke, E. Roldán, and G. J. de Valcárcel, *Appl. Phys. B: Lasers Opt.* **79**, 175 (2004).
- [15] H. Fu and H. Haken, *J. Opt. Soc. Am. B* **5**, 899 (1988).
- [16] E. Roldán, G. J. de Valcárcel, J. F. Urchueguía, and J. M. Guerra, *J. Opt. Soc. Am. B* **20**, 816 (2003).
- [17] R. Paiella *et al.*, *Appl. Phys. Lett.* **79**, 2526 (2001).
- [18] F. Capasso, C. Gmachl, D. L. Sivco, and A. Y. Cho, *Phys. Today* **55**(5), 34 (2002).
- [19] T. Norris (private communication).
- [20] F. Capasso *et al.*, *IEEE J. Quantum Electron.* **38**, 511 (2002).
- [21] L. Diehl *et al.*, *Appl. Phys. Lett.* **88**, 201115 (2006).
- [22] L. Diehl *et al.*, *Appl. Phys. Lett.* **89**, 081101 (2006).
- [23] R. Paiella *et al.*, *Science* **290**, 1739 (2000).
- [24] M. Beck *et al.*, *Science* **295**, 301 (2002).
- [25] The main contribution to the error bars is due to the uncertainty in determining the position of the center of mass of the two lobes present in the optical spectra.
- [26] R. W. Boyd, *Nonlinear Optics*, 2nd ed. (Academic Press, London, 2003).
- [27] F. Salin, J. Squier, and M. Piché, *Opt. Lett.* **16**, 1674 (1991).